

INTELLIGENT SYSTEMS AND APPLICATIONS IN ENGINEERING

ISSN:2147-6799 www.ijisae.org Original Research Paper

A New Approach for Steady-State Calculations and Control of Doubly-Fed Induction Generator Performance Based on the Wind Turbine

Rayane Leulmi^{1*}, Salima Lekhchine², Ammar Medoued³

Submitted: 13/01/2024 **Revised:** 05/05/2024 **Accepted:** 12/05/2024

Abstract: The ecological advantages of renewable energy, especially wind farms, motivate grid integration. The doubly-fed induction generator (DFIG) is the topology most frequently utilized in the industrial sector, which offers improved performance control. Despite all these advantages, several drawbacks have disrupted control and reduced system performance. This system threatens the safety and stability of the wind energy system because of the direct interaction between the grid and DFIG. Therefore, DFIG-based wind systems must conduct a steady-state (SS) evaluation and create control techniques. In this paper, a new modified control strategy for the rotor side of a DFIG is proposed utilizing a mathematical model with a stator magnetization strategy $Q_S = 0$. The stator magnetization strategy aims at an analyzer steady-state of the DFIG to solve the disturbance problem and control all DFIG variables to meet system requirements better. The programming results were validated in the MATLAB environment. System performance shows the effectiveness of the proposed strategy in obtaining a viable model with an error rate of 1.99%. The results validate the programming and enhance the current DFIG's failure analysis, machine performance, steady-state validation, and search efficiency.

Keywords: Wind energy, DFIG, Rotor side converter, Fuzzy logic control, Steady-state control, Performance control.

1. Introduction

Modern society is pushing for the implementation of renewable energies because of the harmful effects of fossil fuels on the environment and human health [1]. Wind power is the most promising of these. Wind energy has a large production capacity and is an excellent alternative to fossil fuels [2]. To maintain ideal conditions, enhance performance, and lessen mechanical stress on the rotor, wind turbine speed can be adjusted by wind conditions when operating at varied speeds [3]. Because of their many benefits over other types, doubly-fed induction generators (DFIG)-driven wind energy conversion systems (WECS) with variable speeds are prevalent [4]. The DFIG stator is directly connected to the grid via a Grid-Side Converter (GSC), while a Rotor-Side Converter (RSC) is a three-phase converter that is connected to the rotor circuit using sliding rings [5]. To maintain allowable voltage changes, the GSC and RSC converters are connected to the capacitor in the intermediate circuit [6]. The most popular renewable energy technology is wind energy based on DFIG, but its grid connection is difficult and challenging [7]. However, this system presents issues and risks to the stability and safety of the WECS due to the direct connection with DFIG and the electrical network.

¹PhD Student, Department of Electrical Engineering, Faculty of Technology, LES Laboratory, University of 20 August Skikda, 21000, Algeria,

rayane.leulmi@univ-skikda. (Corresponding Author)

²Doctor, Department of Electrical Engineering, Faculty of Technology,LGMM Laboratory University of 20 August Skikda, 21000, Algeria

Email: s.lekhchine@univ-skikda.dz

³Professor, Department of Electrical Engineering, Faculty of Technology, University of 20 August Skikda, 21000, Algeria.

Email: amedoud75@yahoo.fr

The characteristics of system behavior that can be acquired in the system include current fluctuations, power losses, and voltage changes. To create a more efficient system, it is therefore required to implement a promising control approach. The growing popularity of DFIG has pushed researchers to explore costeffective control methods. For this reason, numerous studies have been carried out to control the DFIG under steady-state (SS) conditions [8]. Phase diagram analysis is presented in Ref [11], which also computes the power expression under the magnitudephase equivalent circuit and derives the DFIG's steady-state power-angle characteristic. space vector pulse width modulation is used to study DFIG performance using stator flux direction vector control [10]. Ref [12] offers a robust nonlinear controller that maximizes power extraction from WECS while ensuring DFIG stability. Ref [13], An examination that compares the DFIG vector control and sliding mode. In Ref [14] A stability analysis in the steady state at all operating wind speeds. The scientific literature [15] advises calculating the steady-state quantity of the DFIG using exact techniques. Consequently, for DFIG-based wind generation systems, a steady-state evaluation and control strategy development is required [9] and that's our goal in this work. Article [16] analyzes the DFIG's steady-state control strategy using mathematical equations with rotor magnetization $i_{dr} = 0$. In this work, we have presented the same DFIG steady-

state performance analysis strategy as in the paper [16], with a new modified strategy, and from the comparative results we can confirm that the proposed magnetization-controlled DFIG offers better performance. This paper focuses on developing a modified approach for steady-state control of the DFIG via stator flux magnetization $Q_S=0$. The model

studied is based on the control of the 2 MW variable-speed DFIG in a speed range from 900 to 2000 rpm using mathematical equations via stator flux magnetization $Q_{\rm S}=0$. The analysis and

control have been presented in detail, and from the illustrated results it is evident that the suggested approach is highly effective for DFIG control, and its effectiveness has been validated by comparing the results with the best-known vector control model in the synchronous reference frame with the proportional-integral controller. This method is crucial for resolving and preventing faults, as many threaten our DFIG-based wind power systems. According to the table below, simulation results demonstrate the system's efficiency throughout a broad speed scale of 900 to 2000 rpm, with equal steady-state values for two approaches and an error of 1.99%. System reliability demonstrates the effectiveness of the suggested technique in producing a viable model with a 1.99% error rate. We intend to use this work as an initial basis for future failure analysis of systems, especially as it is a faster and more efficient technique than the Simulink model.

2. Wind Energy Conversion System

The most widely used system for wind energy conversion is WECS, which is based on DFIG at variable speed. The stator circuit is directly linked to the grid, but the DFIG rotor circuit is coupled to the grid via a back-to-back voltage source converter which minimizes higher-level harmonics. The system studied comprises a wind turbine, a DFIG, an RSC, and a control unit for the wind turbine, and the DFIG as shown in Figure 1. This topology's main advantage is that it decouples the two converters, enabling them to be independently regulated. To maximize wind energy harvesting and forecast generator performance, a thorough understanding of modeling, control, and steady-state analysis is needed [18].

The DFIG is linked to a continuous frequency power grid with a constant voltage (DC voltage), and MATLAB/Simulink software is used to build the generator control framework. To reach the V_{bus} voltage as a constant voltage, we remove the grid side and fix the DC bus current because this study aims to manage the performance of the DFIG. The control method is predicated on a mathematical model with a stator magnetization strategy $Q_S=0$ calculated by MATLAB coding from the DFIG steady-state equivalent circuit in dq. This novel approach was validated by comparing a model of a three-phase voltage source converter on the rotor side that uses pulse-width modulation switching and a transformation-defined control method inside a synchronous DQ reference frame and an ABC.

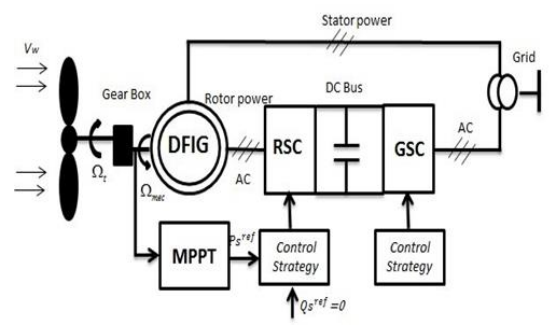


Fig 1. Construction of wind systems based on DFIG

3. Control Strategy For Variable Speed Wind Turbine

Wind turbines require control systems to ensure maximum wind energy and constant turbine speed adaptation to wind speed [19, 20]. This section describes how the Wind Turbine (WT) is operated by a Fuzzy Logic Control (FLC), as shown in the control block in Figure 2. Fuzzification, fuzzy inference, and defuzzification are the three structural elements of the FLC.

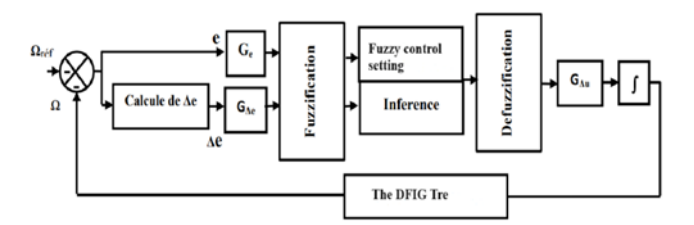


Fig 2. Block schematic of an FLC

Fuzzification is the operation that transforms physical quantities into fuzzy quantities. We have 2 inputs (the error and its derivative) and one output (the control derivative).

• The center-of-gravity method Δ_{un} is given as:

$$\Delta_{un} = \frac{\int x \mu_{(x)}}{\int \mu(x) d_x} \tag{1}$$

Where Δ_{un} is the abscissa of the center of gravity, $\mu(x)$ is the membership function, and x is variable in the universe of discourse.

Control rule: The error and its derivation are functions of the control law $(u = f(e, \Delta e))$. It is provided by:

$$u_{k+1} = u_k + G \Delta_u \Delta_{u_{k+1}} \tag{2}$$

• The derivation of the error and its equivalent normalization are provided by:

$$\begin{cases} x_e = G_e \cdot e \\ x_{\Delta_e} = G_{\Delta_e} \Delta_e \end{cases}$$
 (3)

Where e is the error; Δ_e is the derivation of the error; x_e , x_{Δ_e} is the normalization of error and its derivation; Δ_u is the derivation of control; $G\Delta_u$ is the gain associated with the command u_{k+1} ; $\Delta_{u_{k+1}}$ is the derivation of the command G_e , $G\Delta_e$ are the scaling factors (normalization).

There are several appearance functions, but we've used triangle membership in our study, as represented in Fig 3.

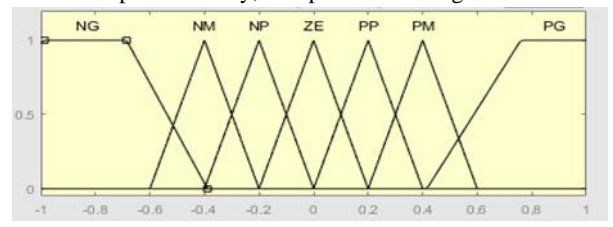


Fig 3. Membership functions (e , Δ_e and Δ_u) used by the FLC

By connecting membership functions to fuzzy rules to generate fuzzy output, fuzzy inference plays a critical role in fuzzy logic operations. Also, employ the max-min approach (Mamdani implication) and the 2D matrix inference rule method. to structure moving from fuzzy to physical quantities (defuzzification). The center-of- gravity approach is shown in Table 1 to calculate the FLC output.

Table 1. Matrix representation

e	NG	NM	NP	ZE	PP	PM	PG
Δe							
NG	NG	NG	NG	NG	NM	NP	ZE
NM	NG	NG	NG	NM	NP	ZE	PP
NP	NG	NG	NM	NP	ZE	PP	PM
ZE	NG	NM	NP	ZE	PP	PM	PG
PP	NM	NP	ZE	PP	PM	PG	PG
PM	NP	ZE	PP	PM	PG	PG	PG
PG	ZE	PP	PM	PG	PG	PG	PG

4. DFIG Performance Control

The major objective of this article is achieved in this section. First, we performed a comparative study between the strategy used in [16] and the proposed modified strategy, then we validated our approach using MATLAB/Simulink models. The following methods are proposed for the SS control of the DFIG in wind turbines:

- Comparison of two magnetization strategies for steady-state DFIG control.
- Using MATLAB/Simulink models to control DFIG performance.

4.1. Control of DFIG performance with both approaches for steady-state calculations

In the event of a failure, system operation can be ensured by applying steady-state control [22]. Steady-state analysis using mathematical equations has become more popular in recent years, as it performs better than simulink results [23]. In this paper, we used a new modified control strategy with a magnetization approach to study the SS performance of the DFIG. Initially, we realized the rotor magnetization method applied in [16], and then our modified approach was realized. According to the results presented, the SS behavior of the machine with stator magnetization is more efficient and robust than the method applied in [16]. For the steady-state analysis, we used DFIG flux vector control of the stator under the dq model [16]. Vector control is the ideal method for steady-state DFIG analysis since it enables us to separate active and reactive power efficiently. Figure 4 shows an equivalent SS circuit in the dq of the DFIG.

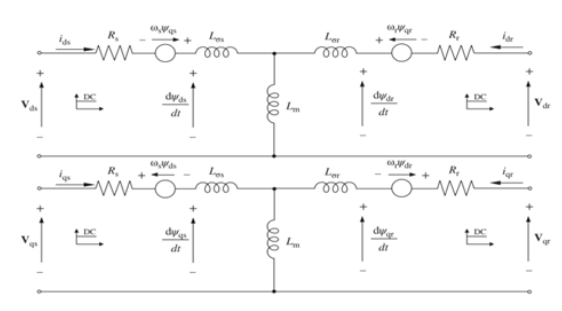


Fig 4. The equivalent SS circuit in dq of the DFIG

a) Magnetization of the DFIG by the rotor: idr = 0

The steady-state analysis of the DFIG in rotor magnetization $i_{dr} = 0$ is performed by the equations summarized in the following equations:

$$\left| \overrightarrow{\psi_S} \right| = \sqrt{\frac{-B \pm \sqrt{B^2 - 4AC}}{2A}}$$
 (4)

With:

$$A = \left[\frac{R_{s}}{L_{s}}\right]^{2} + \omega_{s}^{2} \qquad B = \frac{4}{3} \frac{R_{s}^{T} em^{\omega} s}{p} - \left|\overrightarrow{V_{s}}\right|^{2} \quad C = \left[\frac{2}{3} \frac{R_{s}^{T} em}{pL_{m}}\right]^{2}$$

• Rotor currents:

$$\left|\vec{i}_r\right|^2 = i_{dr}^2 + i_{qr}^2 \tag{5}$$

Where:
$$i_{dr} = 0$$
, $i_{qr} = -\frac{T_{em}}{\frac{3}{2} p \frac{L_m}{L} |\overrightarrow{\psi_s}|}$

Stator currents :

$$\left| \vec{i}_{s} \right|^{2} = i_{ds}^{2} + i_{qs}^{2} \tag{6}$$

With:
$$i_{ds} = \frac{\left|\overrightarrow{\psi_s}\right|}{L_s}$$
, $i_{qs} = -i_{qr} \frac{L_m}{L_s}$

b)Magnetization of the DFIG by the stator: $Q_s=0$

Using the following formulas, we were able to determine the SS values of the DFIG by using the stator to magnetize the generator Os = 0.

Torque :

$$T_{em} = -\frac{3}{2} p \frac{L_m}{L_s} |\overrightarrow{\psi_s}| \tag{7}$$

Stator flux :

$$\left| \overrightarrow{\psi_s} \right| = \sqrt{\frac{-B \pm \sqrt{B^2 - 4AC}}{2A}} \tag{8}$$

Whith
$$A = \omega_s^2$$
, $B = \frac{4}{3} R_s T_{em} \omega_s - \left| \overrightarrow{V_S} \right|^2$

$$C = \left[\frac{2}{3} \frac{R_s}{L_m}\right]^2 \left[\left[\frac{Q_s}{\omega_s}\right]^2 + \left[\frac{T_{em}}{p}\right]^2\right]$$

Rotor fluxes:

$$\left|\overrightarrow{\psi_r}\right|^2 = \psi_{dr}^2 + \psi_{qr}^2 \tag{9}$$

$$\psi_{dr} = L_r i_{dr} + L_m i_{ds}, \ \psi_{ar} = L_r i_{ar} + L_m i$$

Slip:

$$\begin{cases} \omega_r = S.\omega_s \\ \omega_r = \omega_s - \omega_m \end{cases}$$
 (10)

Rotor currents:

$$\left|\vec{i}_r\right|^2 = i_{dr}^2 + i_{qr}^2 \tag{11}$$

Where:
$$i_{ds} = \frac{Q_s}{\omega_s |\overrightarrow{\psi_s}|}$$
, $i_{qs} = \frac{T_{em}}{\frac{3}{2} p |\overrightarrow{\psi_s}|}$

Stator currents :

$$\left|\vec{i}_{s}\right|^{2} = i_{ds}^{2} + i_{qs}^{2} \tag{12}$$

Whith:
$$i_{ds} = \frac{Q_s}{\omega_s |\overrightarrow{\psi_s}|}$$
, $i_{qs} = \frac{T_{em}}{\frac{3}{2} p |\overrightarrow{\psi_s}|}$

Rotor voltages:

$$\left| \overrightarrow{V_r} \right|^2 = V_{dr}^2 + V_{qr}^2 \tag{13}$$

Where: $V_{dr}=R_ri_{dr}-L_r\omega_ri_{qr}+L_m\omega_ri_{qs} \ {\rm and}$ $V_{qr}=R_ri_{qr}+L_r\omega_ri_{dr}+L_m\omega_ri_{ds}$

Stator voltages:

$$\left| \overrightarrow{V_s} \right|^2 = V_{ds}^2 + V_{qs}^2 \tag{14}$$

With: $V_{ds} = R_s i_{ds}$ and $V_{qs} = R_s i_{qs} + \omega_s | \overrightarrow{\psi}_s |$

Stator powers:

$$S_{p} = P_{s}^{2} + Q_{s}^{2}$$
Where:
$$\begin{cases} P_{s} = \frac{3}{2} (R_{s} i_{ds}^{2} + R_{s} i_{qs}^{2} + \omega_{s} | \overrightarrow{\psi}_{s} | i_{qs}) \\ Q_{s} = \frac{3}{2} (V_{qs} i_{ds} - V_{ds} i_{qs}) \end{cases}$$

Rotor powers:

$$R_{p} = P_{r}^{2} + Q_{r}^{2}$$
Where:
$$\begin{cases} P_{r} = \frac{3}{2} (V_{dr} i_{dr} + V_{qr} i_{qr}) \\ Q_{r} = \frac{3}{2} (V_{qr} i_{dr} - V_{dr} i_{qr}) \end{cases}$$

Mechanical power:

$$P_{mec} = \frac{T_{em}\omega_m}{p} \tag{17}$$

Efficiency:

$$\begin{cases} \eta = \frac{P_r + P_s}{P_{mec}} & \text{if } P_{mec} < 0 \\ \eta = \frac{P_{mec}}{P_r + P_s} & \text{if } P_{mec} > 0 \end{cases}$$
(18)

Where, p: the pole pair, L_m , L_s : the self mutual inductances; ψ_s : the magnitudes of flux stator ω_s : the speed of the stator; ω_m : mechanical speed; R_s : the resistance of the stator; V_s : the stator voltage; ω_r : the rotor speed; R_r : the resistance of the rotor; S_p : the apparent stator power; P_s : the active stator power; Q_s : the reactive stator power; S_s : the slip; S_s : the apparent rotor power; S_s : the slip; S_s : the apparent rotor power; S_s : the

active rotor power; Q_r : the reactive rotor power; ψ_{ds} : the flux stator in d-axis; ψ_{qs} : the flux stator in q-axis; ψ_{qr} : the flux rotor in q-axis; ψ_r : the magnitude of flux rotor; ψ_{dr} : the flux rotor in d-axis. i_{qr} is the rotor current in q-axis; V_{qs} : the stator voltage in q-axis; i_{qs} : the stator current in q-axis; V_{qr} : the rotor current in q-axis; V_{dr} : the rotor current in d-axis; V_{dr} : the rotor current in d-axis; V_{dr} :

 V_{ds} : the stator voltage in d-axis.

The performance of the new modified DFIG steady-state control strategy can be examined by performing the programming steps below. The flowchart, shown in Figure 6, describes the programming process applied in the analysis of DFIG performance under steady-state operating conditions using stator magnetization $Q_{\rm S}=0$.

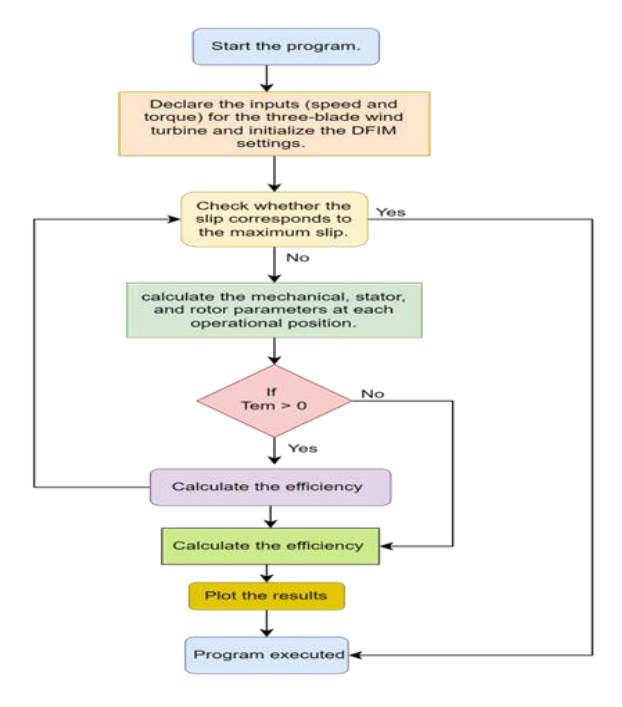


Fig 5. Flowchart of the programming process applied to DFIG performance analysis with $Q_{S}=0$

The steady-state operating strategy can be examined by carrying out the following programming steps:

Step 1: Run the software.

Step 2: Start the DFIG parameters and declare the three-blade wind turbine's inputs (speed and torque).

Step 3: Verify that the slip is equal to the highest percentage of slip

Step 4: Proceed directly to step 10 if this is the case. If not, move on to step five.

Step 5: Determine the mechanical, stator, and rotor parameters at each operation.

Step 6: The operating mode can be identified using the mechanical torque value. In case of a positive torque, proceed to step seven; in case of a negative torque, proceed to step eight.

Step 7: Determine the efficiency of the machine. Proceed to step three after that.

Step 8: Calculate the effectiveness of the DFIG. Proceed to step three after that.

Step 9: Visualize the results of the following variables: rotor currents (I_s , I_r), speed (ω), efficiency (η), and stator and rotor powers (P_r , Q_s and Q_r) electromagnetic torque (T_{em}). Step 10: The program runs successfully.

4.2 Control of DFIG performance using MATLAB/Simulink models

The simulation model in Figure 6 represents WECS based on DFIG. An asynchronous machine with a three-arm universal

bridge converter (RSC) connecting the rotor to a three-phase power source serves as the basis for the DFIG model representation [21]. To simplify the system, We employed a 2-level pulse-width modulation generator to run the RSC and replaced the GSC with a DC voltage supply. At the input of the control block, zero-order blocking was used to operate the system as closely to reality as was practical for rotor angle θ stator voltage (V_S) , rotor speed (ω_m) , and current rotor (I_r) The bus voltage was the same as the DC voltage source. A field-oriented control for the current loops that control the RSC is thought to be the RSC control block.

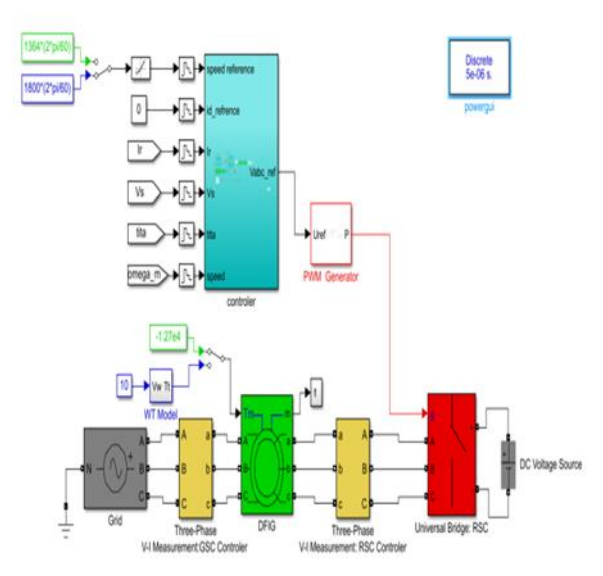


Fig 6. The worldwide wind energy system simulation model

The interior of the RSC control block in the synchronous reference frame is seen in Figure 7. Three proportional integral controllers (PI) are used to accomplish the RSC vector control: a d-axis current controller for the rotor I_{dr} , a speed controller, a q-axis current controller for the rotor (I_{qr}) , and two internal loops for current control that use the required transformation blocks I_{dr} , I_{qr} . A 3rd harmonic injection block raised the output voltage by 15% at the control output. To remove cross-coupling terms, the DC cancellation block was employed. The PI speed controller's output has been multiplied by the gain to get the I_{qr_ref} , while the I_{dr_ref} is maintained at zero. The angle (θ_r) can be computed using the stator voltage (V_{re}) and the angle of the rotor theta. To

provide accurate measurement and rejection of small fluctuations or harmonics, the angle block is used for stator voltage synchronization. The three-phase measurement block and the output measurement signals of the DFIG model were used to obtain the (I_r, V_s) . Using a triangle calibrated between -1 and 1, the regular symmetrical sampling approach is employed in the pulse width modulation (PWM) generator.

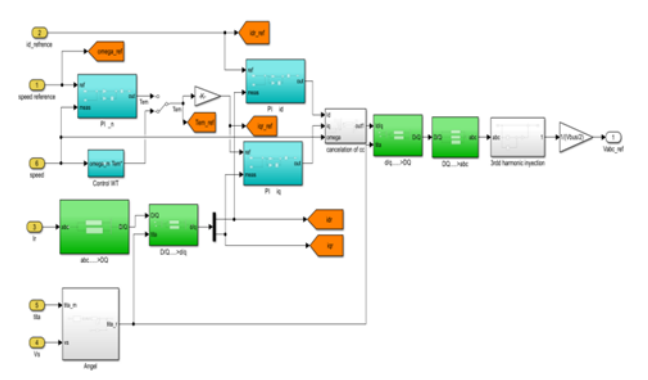


Fig 7. The synchronous frame of reference and its vector control model

4. Results and Discussion

The MATLAB/Simulink platform was used to present the simulation results.

5.1 WT Simulation results

The simulation results studied in the turbine control section were validated in MATLAB/Simulink and presented in Figure 8. From Figure 8.a, we can see that the speed follows its reference perfectly. Figure 8.b shows the aerodynamic power. There is a low static error as shown in Figure 8.c. As a result, the turbine has sufficient reference, tracking, and robustness control. The simulation results show the suggested control's robustness and excellent dynamic performance.

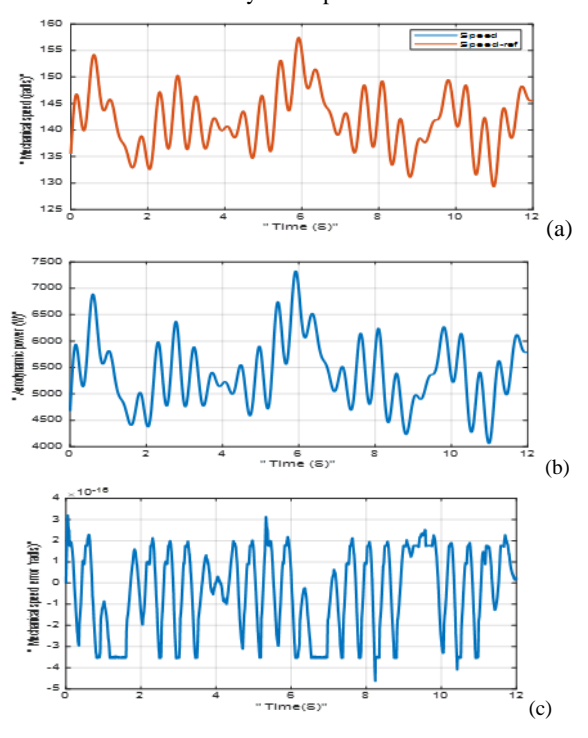


Fig 8. MPPT command simulation with mechanical speed control using FLC.

(a) Mechanical speed, (b) Aerodynamic power, and (c) Error between mechanical speed

5.2 Control results Comparative of both magnetization strategies for steady-state control of DFIG

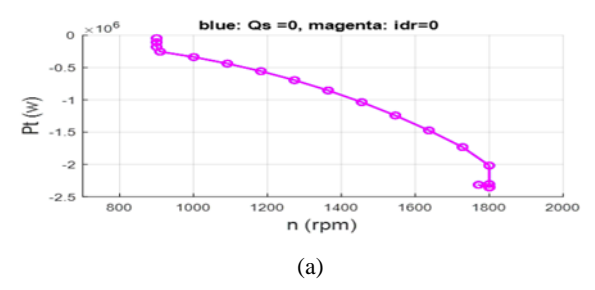
In this section, we present the comparison between the method used in [16] and the new modified strategy. The comparative results are shown in Figure 9. The method used in [16] is shown in magenta $i_{dr} = 0$, while the new modified strategy $Q_S = 0$

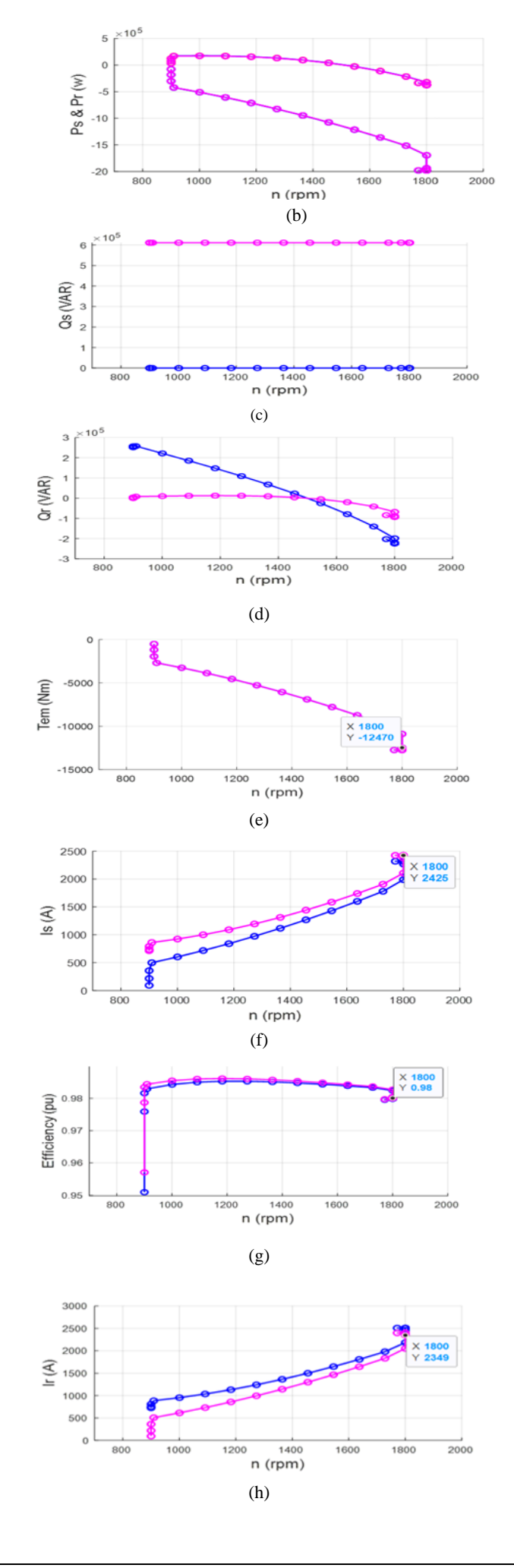
is shown in blue. Figure 9.e, 9.a, 9.i shows that the torque, power, and stator and rotor voltage results are the same regardless of the method used. From Figures 9.e and 9.a there is a proportional relationship between speed and torque and

reactive power resulting from magnetization idr=0 falls with increasing machine speed, and the reactive power arising from stator magnetization is zero as $Q_s = 0$. From Figure 9.d rotor reactive power is dependent upon machine speed, whereas during the stator magnetization phase, the stator reactive power is zero. Figure 9.f demonstrates that the maximum stator current value during $Q_S = 0$ magnetization is less than that during $i_{dr} = 0$ magnetization, whereas Figure 9.h demonstrates that the maximum rotor current value during $Q_S = 0$ magnetization is greater than that during $i_{dr} = 0$ magnetization. Efficiency is the most representative criterion for determining which technique is optimal. It is evident from Figure 9.g that the $Q_S = 0$ magnetization moves more quickly than the $i_{dr} = 0$ magnetization. According to the results presented in [16], at a speed of 1800 rpm, an overall error of less than 10% is observed, according to the calculation of the error between calculated and simulated values, while in this work the error is 1.99%. So we validate that the strategy of magnetizing in the stator is the best and most robust compared to magnetizing By using MATLAB software with varying rotor speeds between 1800 rpm, which is the highest speed, and 900 rpm, which is the lowest, we employed the stator magnetization technique to determine the variables that are most representative of the DFIG in a steady state. Figure 9 displays the entire set of findings from the DFIG steady-state investigation that used the stator magnetization approach. As shown in Figure 9.a, the torque is negative since the machine is operating in generator mode. The rotor's speed as well as the stator and rotor currents are shown to be proportional in Figures 9.c and 9.d. Since mechanical power P_t is the product of torque and speed, it can be seen in Figure 9.e that it takes the same shape as torque. With a maximum active power of about 2 MW, the stator and rotor active power P_s , P_r is displayed in Figure 9.f. The voltages of the stator $(V_{\mathcal{S}})$ and rotor $(V_{\mathcal{T}})$ are displayed in Figure 9.i. Since the stator is directly linked to the power grid, as can be seen, the stator voltage amplitude is constantly constant. Because the stator circuit and the grid are directly connected, we can observe that the stator voltage is constant, whereas the rotor voltage fluctuates and is dependent on the rotor speed. The reactive power of the rotor and stator is shown in Figure 9.g and Figure 9.h. The reactive power of the stator is zero during the stator magnetization phase and that the rotor reactive power decreases as the rotor speed increases.

between speed and power. From Figure 9.c It is clear that the

Figures 9.e and 9.f demonstrate to us that the turbine produces the required torque and power each time the speed rises. DFIG provides the best stator magnetization performance, as seen in Figure 9.b.





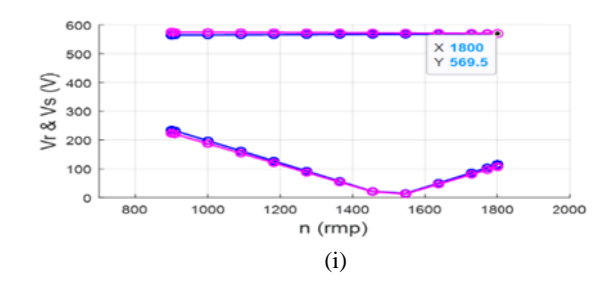
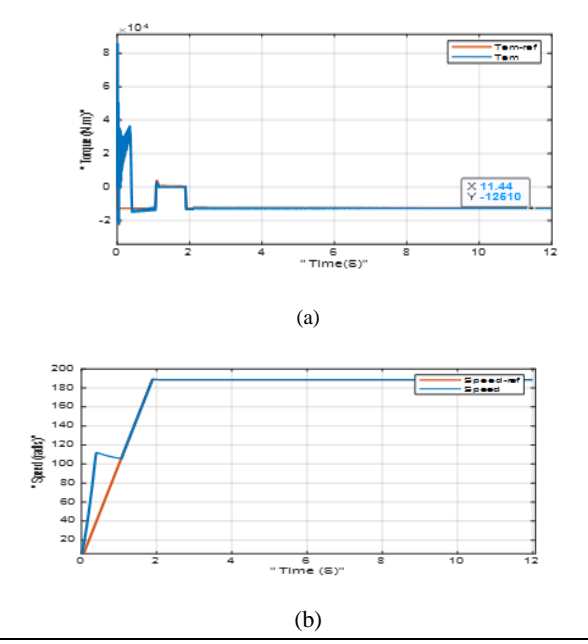


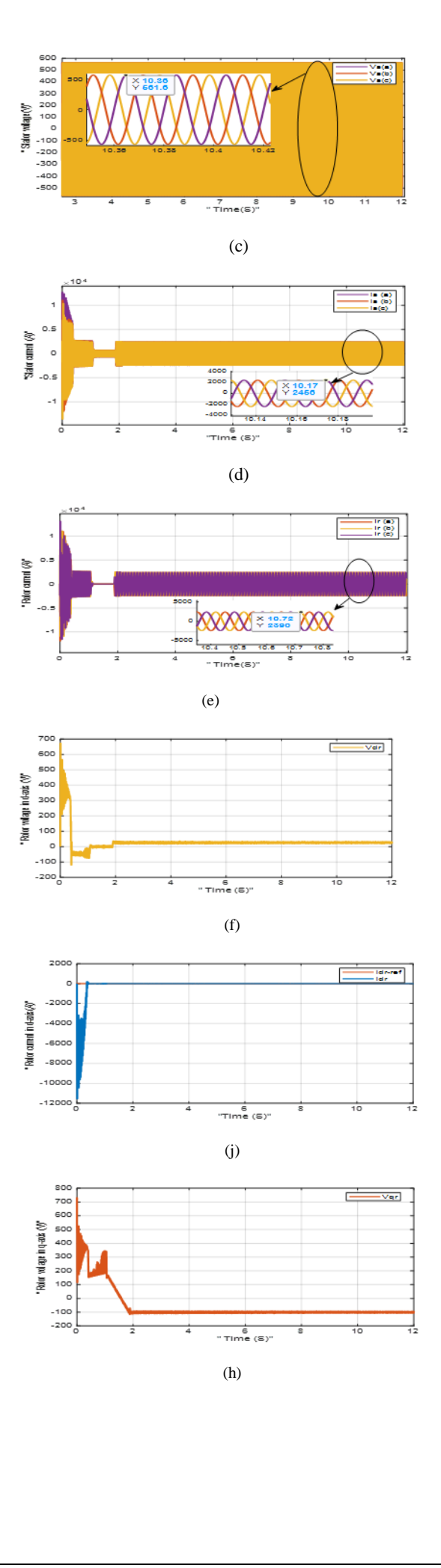
Fig 9. Steady-state control of the DFIG in a variable-speed wind turbine with both magnetization techniques $Q_S=0$ and $i_{dr}=0$. a) Total power; b) Stator and rotor active power; c) Stator reactive power; d) Rotor reactive power Rotor current; e) Torque; f) Stator current; g) Efficiency; h); Rotor current; i) Stator and rotor voltage

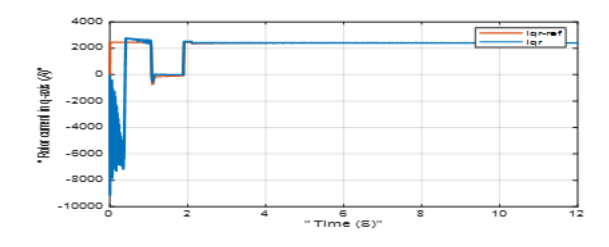
5.3 DFIG performance simulation results using MATLAB/SIMULINK

Figure 10 shows a simulation of the structural DFIG-based wind turbine structure's behavior using MATLAB/SIMULINK. Figure 10 shows torque, rotation speed, stator voltage, stator current, rotor current in the d-axis, rotor voltage in the d-axis, rotor voltage in the q-axis, and rotor current in the q-axis respectively. Given that electromagnetic torque is a function of, Figure 10.a shows that it follows its reference exactly and has the identical form as the q-axis rotor current \boldsymbol{I}_{qr} . As we can see in Figure 10.b, the optimum speed is reached when the transient regime gradually approaches the reference speed and overlays the steady state. Figure 10.c shows that the stator voltage, with an amplitude of 562.4 V, remains constant. We can observe that the currents in the three-phase stator produced by the DFIG are precisely sinusoidal in Figure 10.d. We can observe that the currents are exactly sinusoidal in Figure 10.e, which depicts a three-phase rotor of the DFIG. Since the rotor currents along the q- and d-axes precisely track their references, as shown in Figure 10. j and 10. i, the current I_{dr} is equal to zero as a reference value and I_{qr} maintains the identical torque form. Since our chosen rotor refers to the stator, Figures 10.f and 10.h show that The values of the rotor voltages along the d and q axes are lower. The rotor voltage along the qaxis fluctuates with \boldsymbol{I}_{qr} , and since $\boldsymbol{I}_{dr}=0$, the \boldsymbol{V}_{r} along the



d-axis is equal to zero.





(i)

Fig 10. Results of the DFIG performance study simulation with Simulink/MATLAB models. (a) Torque, (b) Rotation speed, (c) Stator voltage, (d) Stator current, (e) Rotor current, (f) Rotor current (d-axis), (i) Rotor voltage (d-axis), (j) Rotor voltage (q-axis), (k) Rotor current (q-axis)

6. Comparative Control and Discussion

This section compares the method proposed with the Simulink model for the most typical quantities of DFIG. Figure 9.e displays the torque obtained by the steady-state control, which is -12510 N.m., while Figure 10.a shows the torque computed through the Simulink model, which is -12790 N.m. Figures 9.i and 10.c demonstrate that the stator voltage is constant throughout operation. The stator voltage determined through the Simulink model is 563.4 V, whereas the steady-state analysis yields a value of 561.6 V. This makes the comparisons comparable. The system-calculated stator current value in Figures 9.f and 10.d is 2418 A, while the value derived from the equations is 2456 A; the two values fall within similar bounds. A fair comparison of the rotor current levels may be seen in Figures 9.h and 10.e. The value acquired with MATLAB/programming is 2390 A, while the value computed using MATLAB/Simulink is 2389 A for the rotor current. The values acquired by the calculation and simulation, are shown in Table 3 at the operating point, in steady state, with n= 1800 rpm (The percentage decrease over the computed value is represented by \u2214, and the percentage increase above the calculated value is indicated by \↑\). The total error, or 1.99%, is the difference between the simulated and computed values. As a result, the findings verified that the system as intended functions properly and can be utilized for further monitoring in the event of a malfunction.

Table 3. Comparison of steady-state values using the two methods "Operating point is 1800 rpm"

Steady-state	Computed	Simulated	Error (%)	
variables	Values	Values		
Rotor current (A)	2390	2389	0.04 ↑↑	
Stator current (A)	2456	2418	1.56 ↓↓	
Stator voltage (V)	561.6	563.4	0.32 ↓↓	
The couple (N.m)	-12510	-12520	0.07 ↑↑	
	The overall		1.00	
	error		1.99	

7. Conclusion

In this paper, a new mathematical equation-based control technique for analyzing system performance has been devised that makes use of the stator magnetization strategy. Validation of this technique has been verified by implementing a practical control technique on the rotor-side converter using MATLAB/Simulink models. The performance of the proposed system was verified with a comparative study of both techniques, focusing on a speed value of 1800 rpm. The simulations' evaluations confirm good performance and have

proved the effectiveness and reliability of the proposed control. The proposed control strategy a viable model with a 1.99% error rate was produced. Future work aims to use the system developed for detailed analysis of the DFIG based on a wind turbine in the event of failure.

References

- [1] Al-Yozbaky, O. S. A; & Khalel, S. I. 2022. The Future of Renewable Energy in Iraq: Potential and Challenges. *Indonesian Journal Of Electrical Engineering And Informatics* (*IJEEI*), 10(2).
- [2] Sawant, M; Thakare, S; & Rao, A.P. 2021. A Review on State-of-the-Art Reviews in Wind-Turbine- and Wind-Farm-Related Topics. *Energies*, *1.14*(8), 2041.
- [3] Ramalingegowda, C.H; & Rudramoorthy, M.2023. Stability Enhancement of DFIG Wind Farm Using SSSC With FOPID Controller. *Indonesian Journal Of Electrical Engineering And Informatics (IJEEI)*, 11(1).
- [4] Chung, P. D. L. N; & Hieu, T. T. 2023. Optimal operation mode of wind turbines in distribution grid to minimize energy loss considering power generation probability. *Indonesian Journal Of Electrical Engineering And Informatics (IJEEI)*, 11(4).
- [5] Yahdou, A; Benbouhenni, H, & Çolak, İ. 2024. Application of Backstepping Control With Nonsingular Terminal Sliding Mode Surface Technique to Improve the Robustness of Stator Power Control of Asynchronous Generator-Based Multi-Rotor Wind Turbine System. *Electric Power Components And Systems*, 1-29.
- [6] Izanlo, A; Abdollahi, S.E; & Gholamian, S.A. 2020. A New Method for Design and Optimization of DFIG for Wind Power Applications. *Electric Power Components And Systems*, 48(1415), 1523-1536.
- [7] Gianto, R; & Khwee, K.H. 2021. A new T-circuit model of wind turbine generator for power system steady-state studies. *Bulletin Of Electrical Engineering And Informatics*, 14(2), 550-558.
- [8] Rashmi, & Gaonkar, D.N. 2023.. A Novel Approach for Steady State Calculations of VSC-HVDC Connected PMSG Based Offshore Wind Farms Integrated into Multi-Machine Systems. *Electric Power Components And Systems*, 51(10), 961-971.
- [9] Wu, C. P; Cheng, & Ye, Y. 2020. A Unified Power Control Method for Standalone and Grid-Connected DFIG-DC System. *IEEE Transactions On Power Electronics*, 35(12), 12663-12667. [10] Gianto R.2021.. Steady-state model of DFIG-based wind power plant for load flow analysis. *Iet Renewable Power Generation*, 15(8):1724-1735.
- [11] R. Li, X. Yan, and H. Li, "Magnitude-phase equivalent circuit and steady-state power-angle characteristic analysis of DFIG". *International Journal Of Electrical Power & Energy Systems*, Vol. 156, pp. 109767, 2024.
- [12] K.F. Sayeh, S. Tamalouzt, and Y. Sahri, "Improvement of power quality in WT-DFIG systems using novel direct power control based on fuzzy logic control under randomness conditions". *International Journal Of Modelling And Simulation*, pp. 113, 2023.
- [13] D. Babu, and K.R. Bharani, "Investigation on Voltage Stability in a Distributed Generation Power Grid Influenced by PMSG and DFIG Based Wind Energy Conversion System". *Electric Power Components And Systems*, pp. 118, 2023.
- [14] C. Du, X. Du, and C. Tong, "Stability Analysis for DFIG-Based Wind Farm Grid-Connected System Under All Wind Speed Conditions". *IEEE Transactions On Industry Applications*, Vol.

- 59, no. 2, pp. 2430 2445, 2023.
- [15] M. Sharawy, A. Shaltout, and N. Abdel-Rahim, "Simplified Steady State Analysis of StandAlone Doubly Fed Induction Generator". 22nd International Middle East Power Systems Conference (MEPCON), 2021Assiut, Egypt, pp. 246-251.
- [16] Aljafari, B; Stephenraj, J.P; & Indragandhi, V. 2022. Steady State Modeling and Performance Analysis of a Wind Turbine-Based Doubly
- Fed Induction Generator System with Rotor Control. *Energies*, 15(9), 3327.
- [17] Rayane, L; Lekhchine, S; & Medoued. A. 2023, Steady-State Analysis of the Wind Turbine Based on DFIG with Two Different Magnetization Techniques. 14th International Renewable Energy Congress (IREC), Sousse, Tunisia, IEEE Xplore, 1-4,
- [18] Kumar, CVS A; S.S. 2021. Enhanced modelling of doubly fed induction generator in load flow analysis of distribution systems. *Iet Renewable Power Generation*, 15(5), 980-989.
- [19] Vu, N.T; Nguyen, H.D; & Nguyen, A.T. 2022. Reinforcement Learning-Based Adaptive Optimal Fuzzy MPPT Control for Variable Speed Wind Turbine. *IEEE Access*, 10,95771 95780.
- [20] Salem, A.A; Aldin, N.A.N; & Azmy, A.M.2021. Implementation and Validation of an Adaptive Fuzzy Logic Controller for MPPT of PMSG-Based Wind Turbines. *IEEE Access*, *9*, *165690 165707*.
- [21] Cheng, T; Wu, J; & Wang, H. 2023. Dynamic optimization of rotor-side PI controller parameters for doubly-fed wind turbines based on improved recurrent neural networks under wind speed fluctuations. *IEEE Access*, 11, 102713 102726.
- [22] Li, D; Sun, M; & Yong, F. 2021. A General Steady-State Voltage Stability Analysis for Hybrid Multi-Infeed HVDC Systems. *IEEE Transactions On Power Delivery*, 36(3), 1302 1312.
- [23] Varghese, LJ; Jayaraman, R; & Cherukupalli, K. 2023. Performance Analysis of Microgrid Using Wind Power Based on Steady-State Voltage Stability. *Electric Power Components And Systems*, 51(20), 2464 2473.